Investigation of the effects of two Kirchhoff migration algorithms on reflection amplitudes

Zorondras Rodriguez and Gary F. Margrave

ABSTRACT

The effects of seismic migration on reflection amplitudes were tested with two Kirchhoff migration algorithms, one a simple diffraction stack algorithm and the other a full-featured, linear-interpolation Kirchhoff migration. A test acoustic velocity model was constructed and finite difference seismic forward modeling was done on the test velocity model to produce a zero offset section, which was then inverted by the two competing methods. Least-squares scale factors were determined and applied to each image in order to best fit the images to the model reflectivities. The least squares scalars for the two algorithms differed by almost five orders of magnitude, with neither being near unity. After scaling, the amplitudes of key reflectors in the scaled depth converted migrated sections were compared directly to the reflectivity that produced them. The L_2 Norms of the residual of the scaled amplitudes and the reflectivity were compared for key reflection events. The diffraction stack method increases the contrast of the amplitudes between reflectors by 1.53-1.66 times, produces amplitudes that are erratic and uneven across reflectors as a function of position, and is highly sensitive to abrupt lateral changes in reflectivity. However the Kirchhoff migration algorithm decreases the contrast between amplitudes by 1.48-3.09 times, produces amplitudes which are fairly uniform and constant with respect to position along a reflector, and is also sensitive to abrupt lateral changes in reflectivity. Additionally comprehensive quantitative amplitude comparison and analysis test methodology was developed and described and is applicable to the testing of other varieties of migration algorithms. Finally two new CREWES MATLAB utilities **vz2vt**, and **mig2depth**, were developed to complete the testing, and are described.

INTRODUCTION

Post-stack migrated reflection amplitudes are routinely used in industry to evaluate prospective drilling locations. The accuracy of these amplitudes, and in particular the accuracy of their contrast, is crucial to making informed drilling decisions. However, equally important is knowledge of the target's position, and both amplitude control and spatial positioning are key goals of seismic migration.

Kirchhoff migration is a standard method of seismic migration used in industry. However, true reflection amplitudes are often obscured in the imaging processes due to different weighting and interpolation schemes used by competing algorithms.

This study compares two different algorithms of Kirchhoff migration, namely a simple diffraction stack, and a more advanced implementation of Kirchhoff migration, in order to quantify the effects of weighting and interpolation on the amplitudes of a migrated section. In the process, several amplitude comparison techniques were developed. This study was conducted using the CREWES 2006 MATLAB toolbox; however, the techniques developed will also be used in the future to evaluate industrial codes.

In order to make comparisons of the effects of the different algorithms, a velocity model was constructed and a zero-offset section (ZOS) exploding reflector image was generated by finite difference modeling. This ZOS image was then inverted by the two competing time-migration algorithms to produce a diffraction stack image and a Kirchhoff migration image. These images were then converted to depth, and scaled in the least squares sense to the reflectivities that produced them. Finally the amplitudes of the reflection events in each image were then quantitatively compared to the reflectivities expected from the velocity model. This test methodology hence requires a method of computing the expected reflectivity from a given model, and two such methods were explored. Finally two new CREWES MATLAB utilities were developed to complete the testing, these tools are **vz2vt** a program that re-samples the depth velocity model to a time velocity model, and also outputs a smoothed velocity model in time, and **mig2depth**, which converts a time section into depth given a velocity model in time.

FINITE DIFFERENCE MODELING

The CREWES finite difference modeling toolbox was used to generate the ZOS image used in the inversions. The CREWES finite difference toolbox includes the programs **afd_vmodel** which generates velocity models, **afd_reflect** which calculates a matrix of approximate normal incidence reflectivities from a velocity model, and **afd_explode** which generates a ZOS image of the velocity model. The tools are described in Margrave (2003, pp 52-57).

Finite difference forward modeling seeks discrete solutions to the scalar wave equation, given by

$$\nabla^2\Psi(x,z,t) = \frac{\partial^2\Psi(x,z,t)}{\partial x^2} + \frac{\partial^2\Psi(x,z,t)}{\partial z^2} = \frac{1}{v^2(x,z)}\frac{\partial^2\Psi(x,z,t)}{\partial t^2}, \qquad (1)$$

where $\Psi(x,z,t)$ is the scalar wave field and $v(x,z)$ is the instantaneous velocity from the velocity model. Equation 1 models the propagation of acoustic waves.

THE VELOCITY MODEL

An acoustic velocity model v(x,z) (Figure 1) was created using the CREWES MATLAB utility **afd_vmodel.** This model while relatively simplistic contains two dipping contacts representing either angular unconformities or faulted horizons. It also contains a channel feature, and a broad rounded anticline fold with steeply dipping limbs on either end.

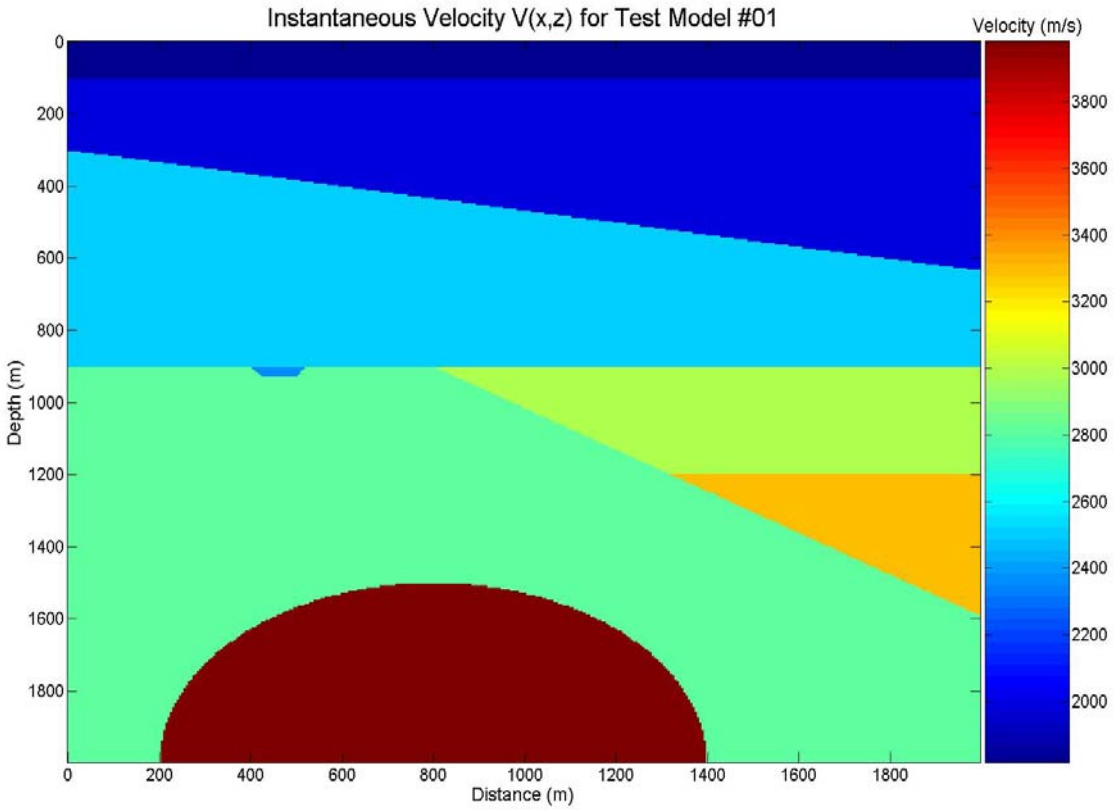

FIG. 1. Test Model #01 instantaneous acoustic velocity matrix.

NORMAL INCIDENCE REFLECTIVITY

Normal incidence reflectivity at an interface between two acoustic media is defined as, (e.g. Margrave, 2005, p1-22)

$$R_{1,2} = \frac{I_2 - I_1}{I_2 + I_1} \tag{2}$$

where

$$I_j = \rho_j \alpha_j \qquad j = 1,2 \ , \tag{3}$$

and where I_1 is the acoustic impedance on the top side of the interface and I_2 is the acoustic impedance on the lower side of the interface, ρ the density and α the acoustic velocity of each medium as denoted by the subscript.

A program to compute a reflectivity matrix using the above equations was implemented as **norm_reflect**. The program **norm_reflect** is capable of also including a density model, however for our models we assume a constant uniform density ρ=1 kg/m^3 for all points in the model matrix. The normal incidence reflectivity R(x,z) of test velocity model #01 is seen in Figure 2.

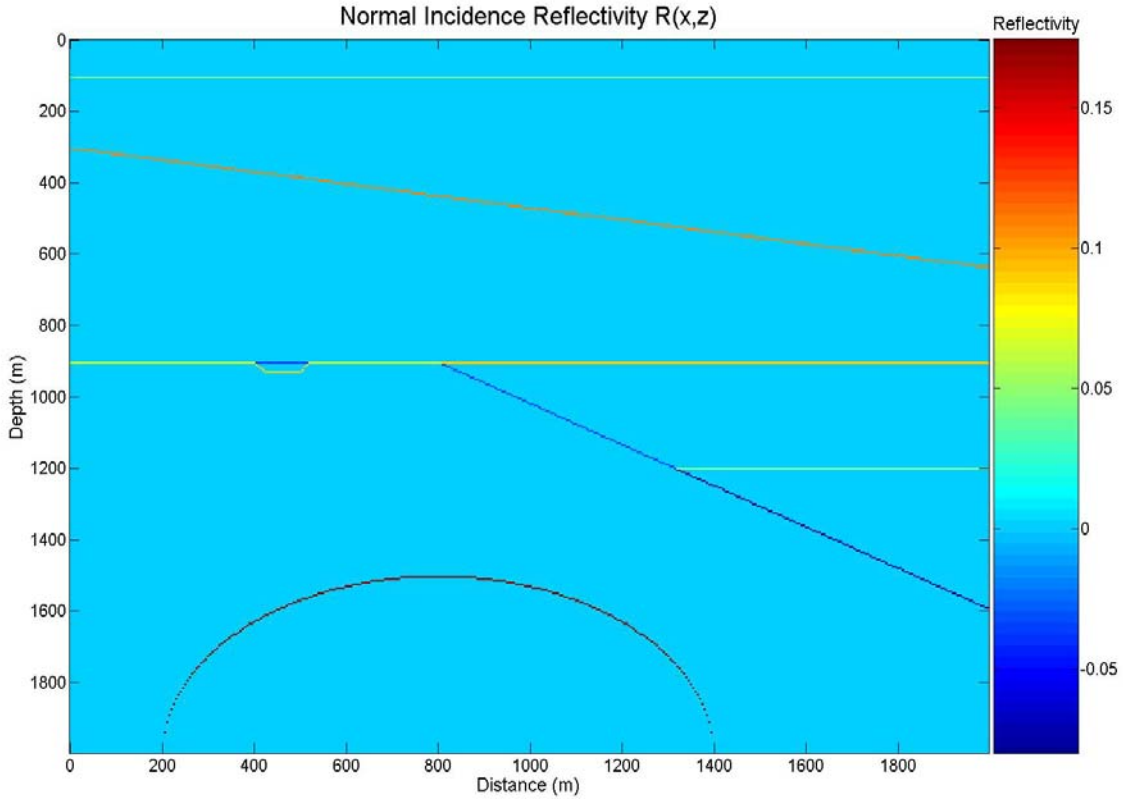

FIG. 2. Normal Incidence Reflectivity R(x,z). Color bar is reflectivity.

GRADIENT REFLECTIVITY

The gradient reflectivity of a continuous impedance model can be approximated by

$$R(x,z) \approx \frac{1}{2} sign\left(\frac{dI(x,z)}{dz}\right) \left|\nabla \log(I(x,z))\right| \Delta x \Delta z \qquad (4)$$

Equation 4 is implemented by the CREWES MATLAB program **afd_reflect**. All finite difference modeling and inversion done in this work was based upon the gradient reflectivity program **afd_reflect**.

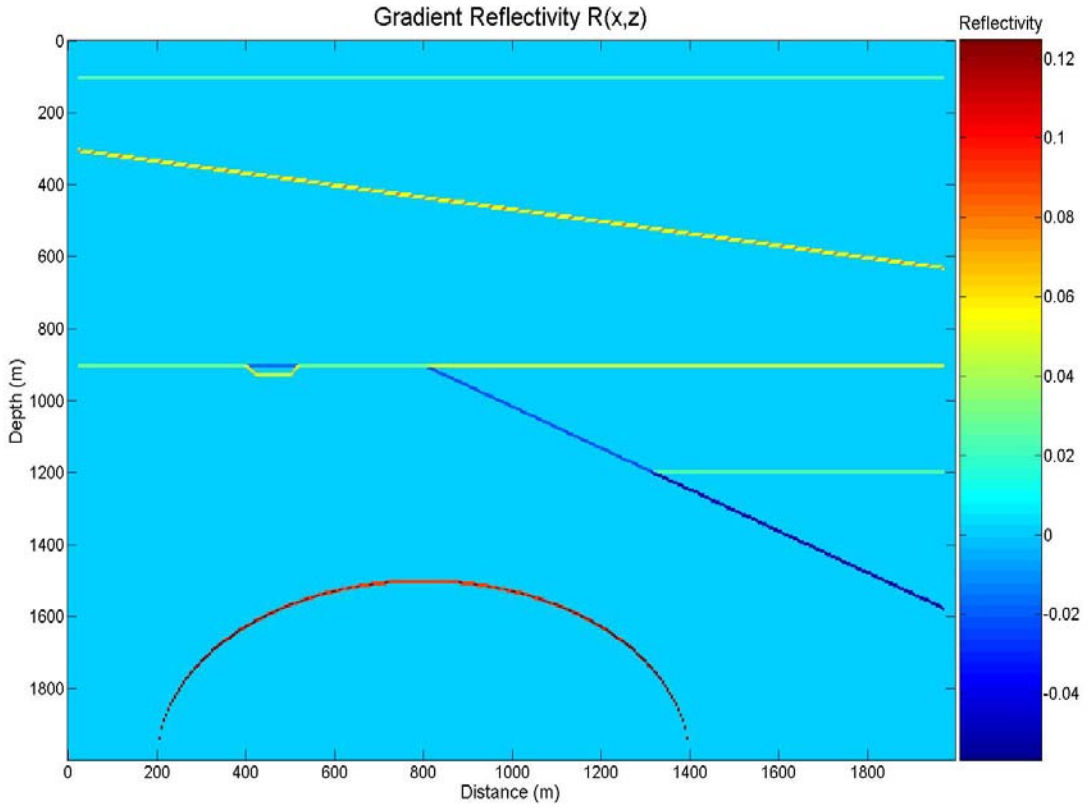

FIG. 3. Gradient Reflectivity of Test Velocity Model #01.

EXPLODING REFLECTOR SEISMOGRAM

The exploding reflector ZOS image of the test velocity model was computed with the finite difference utility **afd_explode**, and is seen below in Figure 4. It is this image that we attempted to invert by Kirchhoff migration and the diffraction stack method.

The idea behind the exploding reflector model, is that each reflection point of non-zero reflectivity will act as the source of a wave at time $t = 0$. Namely a wave will propagate from every reflection point, and the superposition of these wave sources creates a wavefront which propagates to the surface. The amplitudes and of the wavefronts will be recorded by geophones as they reach the surface. Since this is -way propagation, the velocities will be slowed by a half to simulate the two way travel time to each reflection point.

The exploding reflector model (ERM) yields an image which very nearly approximates the image of a zero offset stack section (ZOS) (Margrave, 2003, pg 133). At the time of explosion the wavefield has the shape of the geology. This is the idea that is used in wavefield marching migration algorithms which seek to march the wavefield backwards from the surface in order to determine the original shape of the geology. However for our purposes we will consider it to be a close approximation to an NMO (Normal Move-Out) corrected stacked seismic section. The wave propagation in this case is calculated by time stepping at each point, using an initial wavefield snapshot of zero or no explosion followed by a secondary snapshot of explosions at the positions of

the reflectors. These impulsive sources at the reflector positions are scaled by the reflection coefficients and the next wavefield snapshot is calculated by finite difference.

For our modeling we used a 9-point Laplacian operator, a time stepping of Δt=.0005s, and a horizontal grid spacing of Δx=5m and a sample rate of 5 ms. The exploding reflector model of the test velocity model is seen in Figure 5 below.

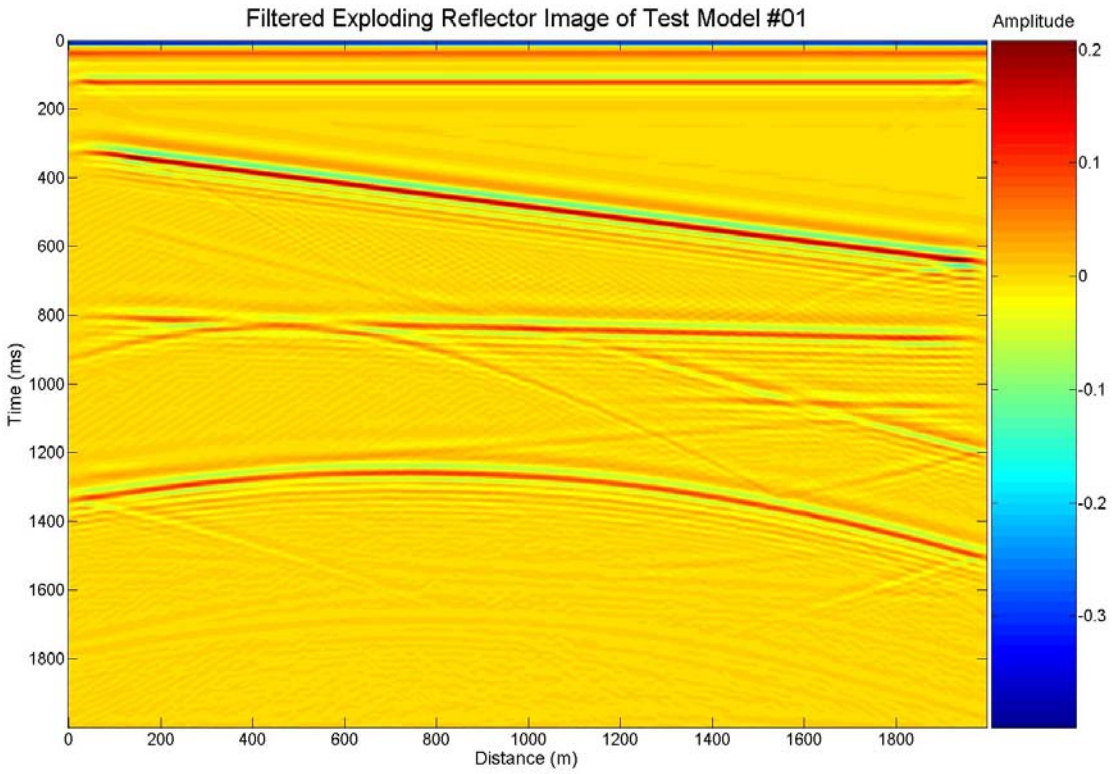

FIG. 4. Exploding reflector model of the test velocity model. Filtered with an Ormsby [10,15,50,60] wavelet. 9-point Laplacian, .0005s sample rate, 5m horizontal grid spacing. Colorbar is amplitude.

RESAMPLING V(X,Z) TO V(X,T) AND RMS VELOCITIES

In order to do either the Kirchhoff migration or the diffraction stack migration, it was necessary to have RMS velocities in time defined for all points in the ZOS image matrix. Since the ZOS image is in time and horizontal distance and the test velocity model is in depth and horizontal distance, the velocity model was resampled from a depth model $v(x,z)$ to a time model $v(x,t)$. RMS velocity is defined as (e.g. Margrave, 2005)

$$V_{rms}(\tau)^2 = \frac{1}{\tau}\int_0^{\tau} v_{ins}(t)^2\, dt \qquad (5)$$

Equation 5 is performed on each column of the time resampled velocity matrix with the CREWES utility **vint2vrms** to create a $V_{rms}(x,\tau)$ matrix. This RMS velocity field is shown in Figure 5 below.

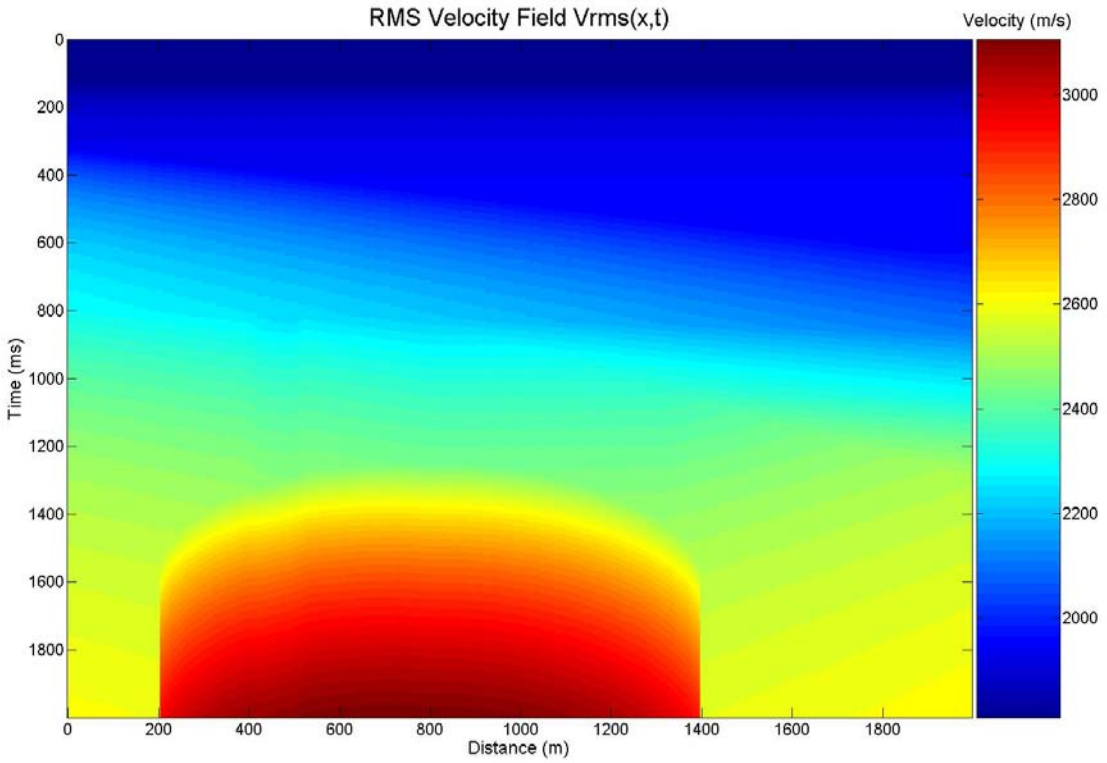

FIG. 5. RMS velocity field $V_{rms}(x,\tau)$ for test velocity model #01.

This smoothed velocity model in time was computed with a newly developed MATLAB utility named **vz2vt**.

SCATTER POINTS AND COMMON DEPTH POINT TRAVEL TIMES

A subsurface scatter point, or scatterer, is a differential element with reflectivity, which upon the arrival of an incident wavefront the element scatters the wave energy in all directions as depicted in Figure 6.

If the scatter point is located in a homogenous half space then wavefronts are spherical and this energy is backscattered along the straight ray paths shown in Figure 7. The amplitude of the backscattered energy depends on the reflectivity of the scatter point and the length of the travel path due to spherical spreading, which is proportional to the inverse of the travel path length. The reflectivity of the scatter point for normal incidence is modeled as in Equation 2, but for other angles of incidence may be modeled using the Zoeppritz equations for plane waves (e.g. Krebes 2006). However for our modeling and inversion the gradient reflectivity of Equation 4 suffices.

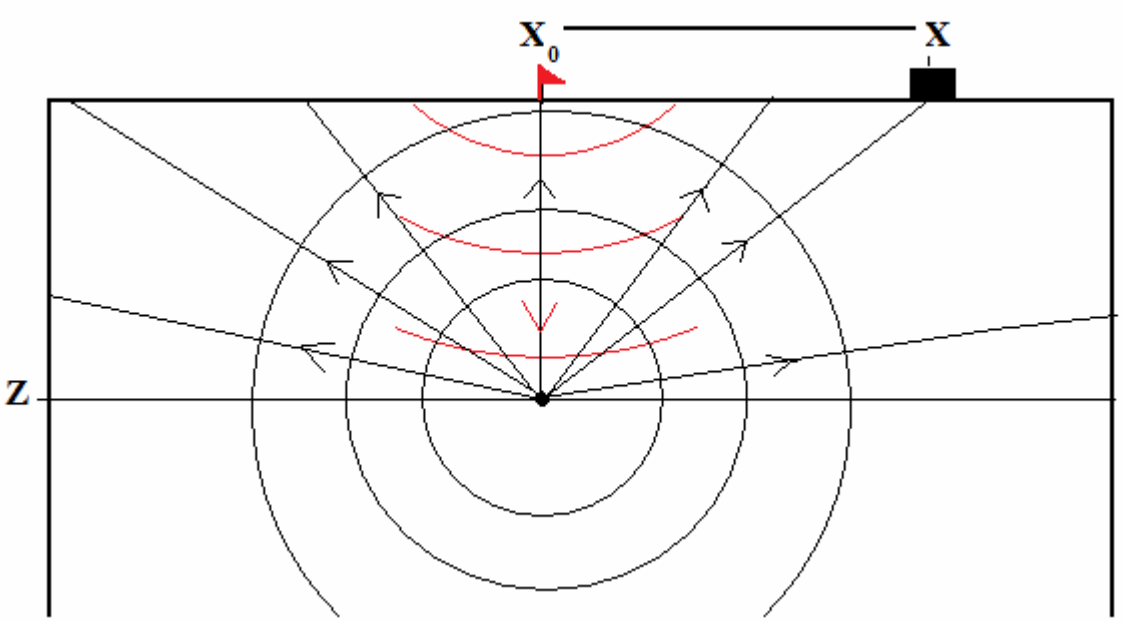

FIG. 6. Diagram of a single scatter point and reflected energy.

Such a scatter point may be thought of as a common depth point (CDP) for the energy that arrives to the surface along each of the scattered wave paths and recorded by geophones. The two-way traveltime of these waves along a ray path with half-offset x and depth z and centered at position x_0 in a homogenous half space with acoustic velocity v is given by the travel time equation

$$T(x-x_0)^2 = T_0^{\,2} + \frac{4(x-x_0)^2}{v^2} \tag{6}$$

where

$$T_0 = \frac{2z}{v} \tag{7}$$

is the vertical two-way travel time.

In the case of vertically heterogeneous, laterally homogeneous media, wavefronts do not follow straight ray paths but rather curved Snell's law ray paths. In this case we may imitate the Snell's Law traveltimes by imagining a fictitious wavefront that travels along a straight line path from the scatter point to the receiver at a suitable replacement velocity. The most suitable velocity for a replacement velocity is the RMS velocity which gives us

$$T(x-x_0)^2 = T_0^{\,2} + \frac{4(x-x_0)^2}{V_{rms}(T_0)^2} \tag{8}$$

If the media is vertically and laterally heterogeneous horizontal slowness is no longer constant and wave fronts follow more complicated paths. However in this case we

approximate the travel time again by using Equation 8 as a reasonable approximation only with $V_{rms}(T_0)$ replaced by $V_{rms}(x_0, T_0)$, i.e.

$$T(x-x_0)^2 = T_0^2 + \frac{4(x-x_0)^2}{V_{rms}(x_0,T_0)^2} \tag{9}$$

DIFFRACTION STACK AND KIRCHHOFF TIME MIGRATION

If we consider reflection surfaces as collections of scatter points, then the signal recorded at the surface may be modeled as a superposition of backscattered waves arriving at the geophone from each scatter point at times given by Equation 9. All of the scatter points with rays which arrive at x with travel time τ sum to give the amplitude $A(x,0,\tau)$. Hence the true amplitude $A_0(x_0,z)$, which is the reflectivity at this point, has been spread out on a diffraction hyperbola. These spread out amplitudes are then summed by superposition with the other hyperbolae crossing these points.

To reconstruct the original reflectivity at position (x_0,T_0) in the ZOS image by inversion we need to build a diffraction hyperbola specified by Equation 9 and go to each point on the curve and without knowing the reflectivity $A_0(x_0,T_0)$, somehow extract it from each superposition sample.

However, not all points on the diffraction curve will coincide with a sample point, so we must also interpolate a value for the curve by using the samples nearby to it. This may be done in a variety of ways from nearest neighbor interpolation to linear or cubic spline interpolation.

Next we make an educated guess of how much of that sample belongs to the diffraction curve associated to (x_0,T_0). This is done by weighting how much of that sample we take or perceive to be part of the diffraction event associated to (x_0,T_0). The sum of all of these spread out pieces should then add up to the desired value of the reflectivity $A_0(x_0,T_0)$. Although there is no way to know how much of the amplitude of the sample selected represents what was contributed by the particular diffraction curve corresponding to reflectivity A_0. A common weighting used to for this is the cosine weighting (Bancroft, 2005)

$$\frac{T_0}{T(x-x_0)} \tag{10}$$

One must be aware that a simple diffraction summation will not approximate the reflectivities properly for dipping reflectors as it is well known that the proper weights are dip dependent. The above ideas were implemented in a program named **difstack.m** using the cosine weighting and nearest neighbor sample interpolation. This program was implemented using pseudo code found in (Bancroft, 2005, p 4.14).

This simple method was tested against the post-stack Kirchhoff time migration routine **kirk_mig**, as developed by Xinxiang Li, J.C. Bancroft and G.F. Margrave (1996), which is a migration utility in the CREWES MATLAB toolbox.

DEPTH CONVERSION OF TIME MIGRATED IMAGES

In order to make comparisons between the gradient reflectivity matrix and the migrated images each image was converted from time into depth using a newly developed MATLAB utility named **mig2depth**. This conversion from time to depth was done on a trace by trace basis using the resampled instantaneous velocity $V(x,t)$ matrix of in accordance with vertical traveltimes, where the time depth conversion depends on the following equation (Margrave, 2005, pg 6-7),

$$z(\tau) = \int_0^{\tau} V_{ins}(t)dt \approx \sum_0^{\tau} V_{ins}(t) \cdot dt \tag{15}$$

This depth section was subsequently windowed to a maximum depth of 2000m by discarding samples below this depth as extraneous.

LEAST-SQUARES MINIMIZING SCALAR

Initially both the seismic image of the Kirchhoff time migrated depth converted section and the depth converted diffraction stack time migrated image have amplitudes which are well outside of the interval [-1, 1] that characterizes reflectivity. In order to compare amplitude results between the two images and the gradient reflectivity matrix, a least squares scalar λ was determined which minimizes the following equation

$$\left\| R(x,z) - \lambda\, \Psi(x,z) \right\|^2 = \iint_{R^2} (R(x,z) - \lambda\, \Psi(x,z,0))^2\, dx\, dz \tag{16}$$

where $R(x,z)$ is the reflectivity matrix and $\Psi(x,z)$ is the seismic image to be scaled.

For a discrete matrix Equation 16 may be approximated as

$$\left\| R_{i,j} - \lambda\, \Psi_{i,j} \right\|^2 = \Delta x\, \Delta z \sum_{i=1}^{M} \sum_{j=1}^{N} (R_{i,j} - \lambda\, \Psi_{i,j})^2 \tag{17}$$

for two M x N matrices $\Psi_{i,j}$ and $R_{i,j}$ representing the discrete versions of the continuous scalar fields $\Psi(x,z)$ and $R(x,z)$. The scalar λ which minimizes Equation 17 is easily derived upon differentiating equation 17 with respect to λ and setting the derivative equal to zero. This least squares scalar is found to be

$$\lambda = \frac{\sum_{i=1}^{M}\sum_{j=1}^{N} R_{i,j} \cdot \Psi_{i,j}}{\sum_{i=1}^{M}\sum_{j=1}^{N} \Psi_{i,j}^{2}} \tag{18}$$

The scale factor λ was determined from windowed versions of each migrated matrix upon comparison with the gradient reflectivity matrix, and then applied as the minimizing bulk scalar in order to approximately compare these amplitudes to the reflectivities that produced them. The least-squares minimizing bulk scalar for the Kirchhoff time migration image matrix was determined to be 318.04, and the least squares minimizing bulk scalar for the diffraction stack image was determined to be 0.02389. These scalars were then applied to each image matrix to scale the amplitudes into the range of the gradient reflectivity for comparison and analysis. The least-squares scaled depth converted Kirchhoff time-migrated image of the exploding reflector model is seen in Figure 7, while the diffraction-stack, time-migrated, least-squares scaled image of the exploding reflector model is seen in Figure 8 below.

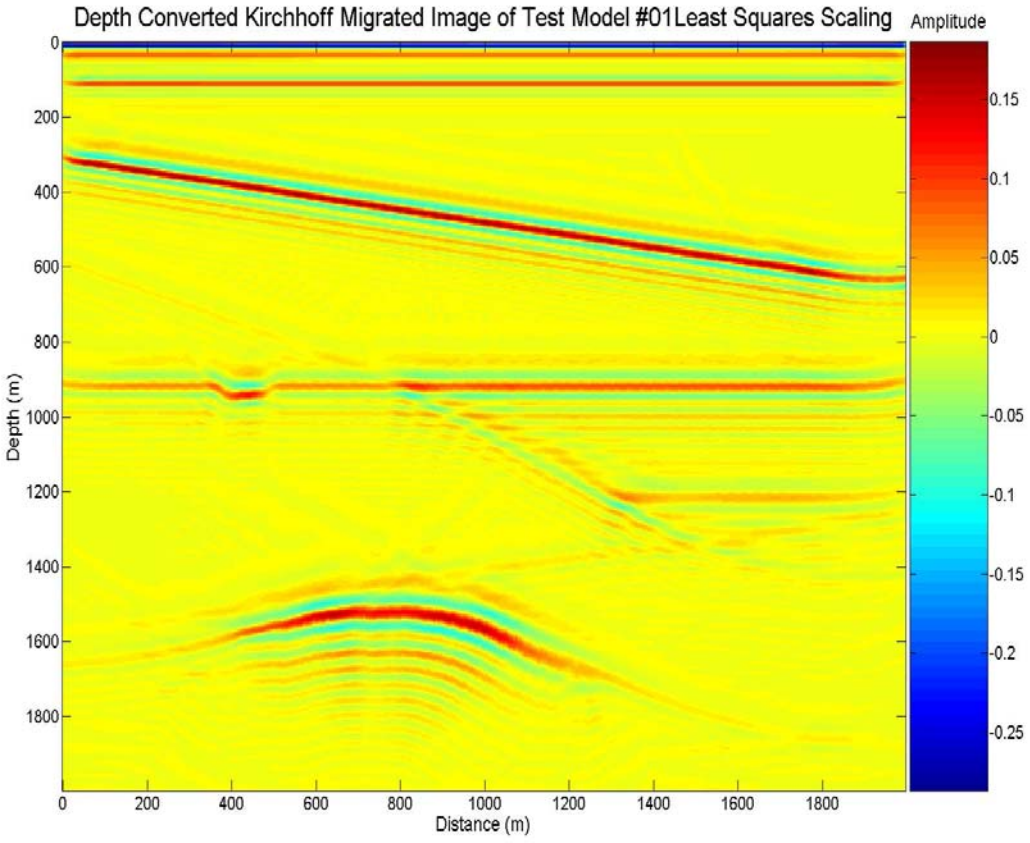

FIG. 7 Depth converted Kirchhoff Migration with least squares scaling.

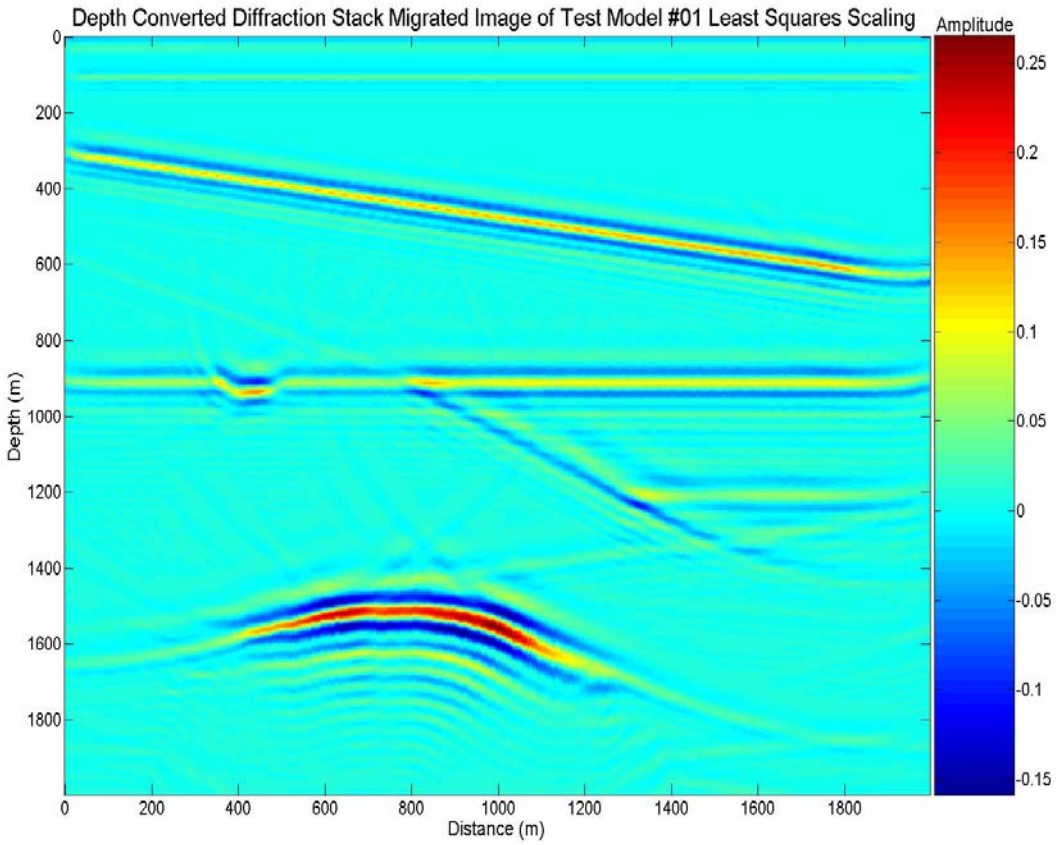

FIG. 8. Depth converted diffraction stack migration with least squares scaling.

QUALITATIVE ANALYSIS OF MIGRATION IMAGES

It is immediately clear from these images upon comparison with the gradient reflectivity image that the Kirchhoff image has values which throw off the linear scaling and cause the image to look yellow. These large negative values which are near surface migration artifacts can be seen as the blue strip across the top of the matrix near a depth of zero. Upon discarding the first 10 rows of each matrix the differences in amplitudes become much clearer. A side by side comparison to reflectivity is seen in Figure 9. This reveals that the contrast between reflectors in the diffraction stack image seems to be more accurate than that displayed in the Kirchhoff migration image. In particular we see that the first horizontal and second dipping reflection event appear to be too strong in the Kirchhoff image and just right in the diffraction stack image as compared with the reflectivity.

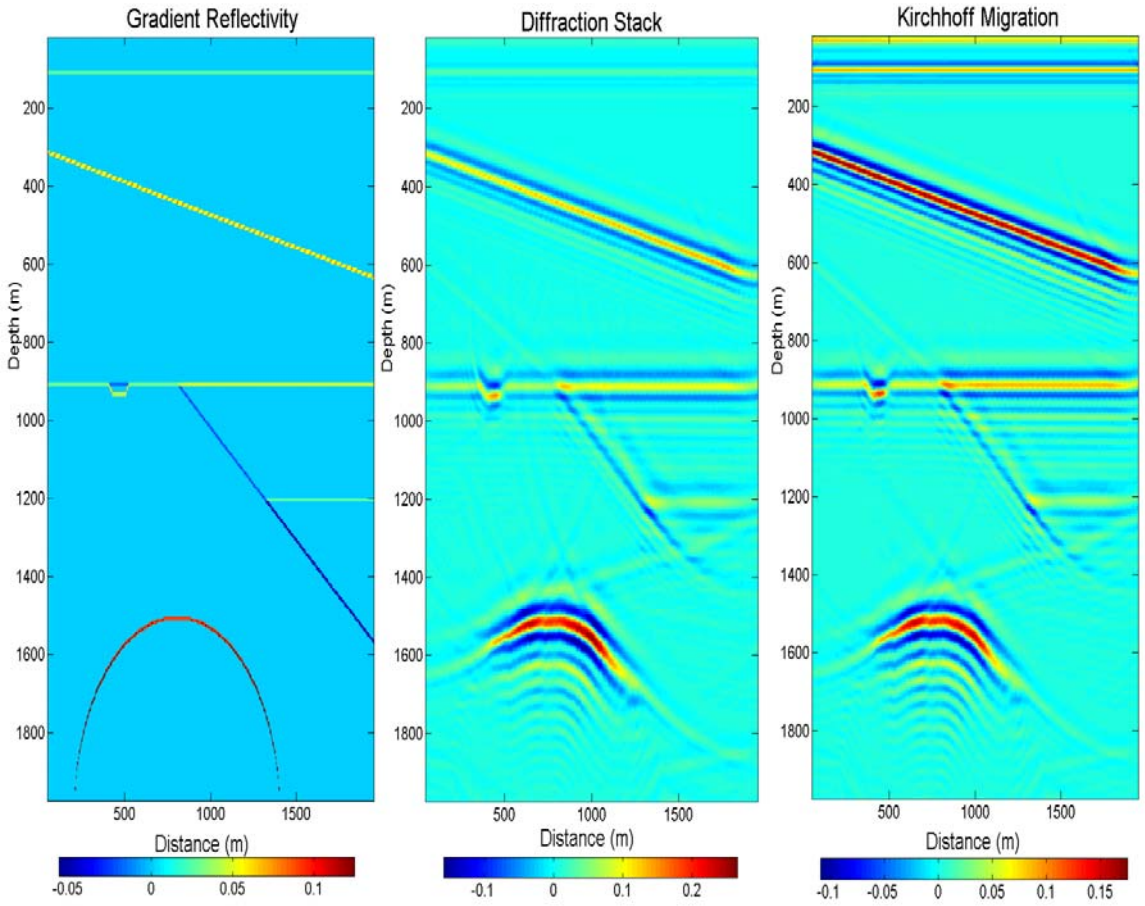

FIG. 9. Side by side comparison of migration images with reflectivity matrix, the first 10 rows of each matrix have been discarded and the positions of the reflectors depth matched to the reflectivity matrix. color bar is reflectivity.

QUANTITATIVE ANALYSIS OF MIGRATION IMAGES

In order to quantitatively compare the amplitude results from each image with the gradient reflectivity, amplitude slices were made through the first horizontal reflector, the 2nd dipping reflector, the 3rd horizontal reflector containing the channel feature and laterally varying reflectivity, and finally through anticline reflector were made. Peak amplitudes from each slice matrix were then extracted for comparison to the reflectivities and the norm of the residual calculated. These slices and plots of the peak amplitude extractions are seen in Figure 10 to Figure 16 below.

In Figure 11 we see the reflectivity estimates from the first horizontal reflector. Here we see that the amplitudes of the scaled diffraction stack image fit the gradient reflectivity values closely, whereas the Kirchhoff migration amplitudes fit further away. We also see that the amplitudes of the Kirchhoff migration image along this reflector are smooth and constant whereas there are fluctuations from the mean along this reflector in the diffraction stack image.

In Figure 13 we see the reflectivity estimates from the peak samples of the 2nd reflector. We see bandlimited estimates of the bimodal reflectivity displayed along this

reflector in both the Kirchhoff and diffraction stack reflectivity estimates. Once again the Kirchhoff migration reflectivity estimates remain more constant as a function of position than the diffraction stack estimates which seem to increase in magnitude down dip. Both estimates drop off rapidly towards either end of the section as the aperture effect truncates the diffraction energy that would need to be summed to produce proper reflectivity estimates. However this aperture effect is more dramatic down dip than it is near the shallower end of the dipping reflector due to truncation.

In Figure 15 we see the reflectivity estimates from the 3rd reflector which contains a lateral drop in impedance at about 400m and a lateral increase in impedance at around 800m. Both the Kirchhoff and diffraction stack reflectivity estimates seem to do equally as well here, with the Kirchhoff estimates being slightly closer to the true reflectivity. However it is interesting to note the large deviation of both estimates from the reflectivity near the two discontinuities. This large excursion seems to suggest that both methods are sensitive to abrupt lateral changes in reflectivity.

Finally in Figure 17 we see the reflectivity estimates taken from the anticline reflector. These extractions were taken from the maximum amplitudes from each column from the slices from Figure 16. Here we see that the Kirchhoff reflectivity estimates better fit the values from the gradient reflectivities than do the diffraction stack reflectivity estimates.

In order to quantify the closeness of fit between the amplitudes along each reflector in migration images and the gradient reflectivity, the residual or difference between the two values was taken and the L_2 norm of these residuals determined. This data is collected below in Table 1. If the fit was perfect the residual would have zero length so in the best case an L_2 norm of zero would be found.

Table 1. L_2 norm of the residual between peak amplitudes the gradient reflectivity values along each reflector.

	Kirchhoff Norm of Residual	Diffraction Stack Norm of Residual
Reflector 1	1.45157	0.14919
Reflector 2	1.92391	1.22319
Reflector 3	0.72990	1.01753
Reflector 4	0.65713	1.39280

From Table 1 we see that the gradient reflectivity is closer fit along reflectors 1 and 2 by the diffraction stack amplitudes, and closer fit along reflectors 3 and 4 by the Kirchhoff migration amplitudes.

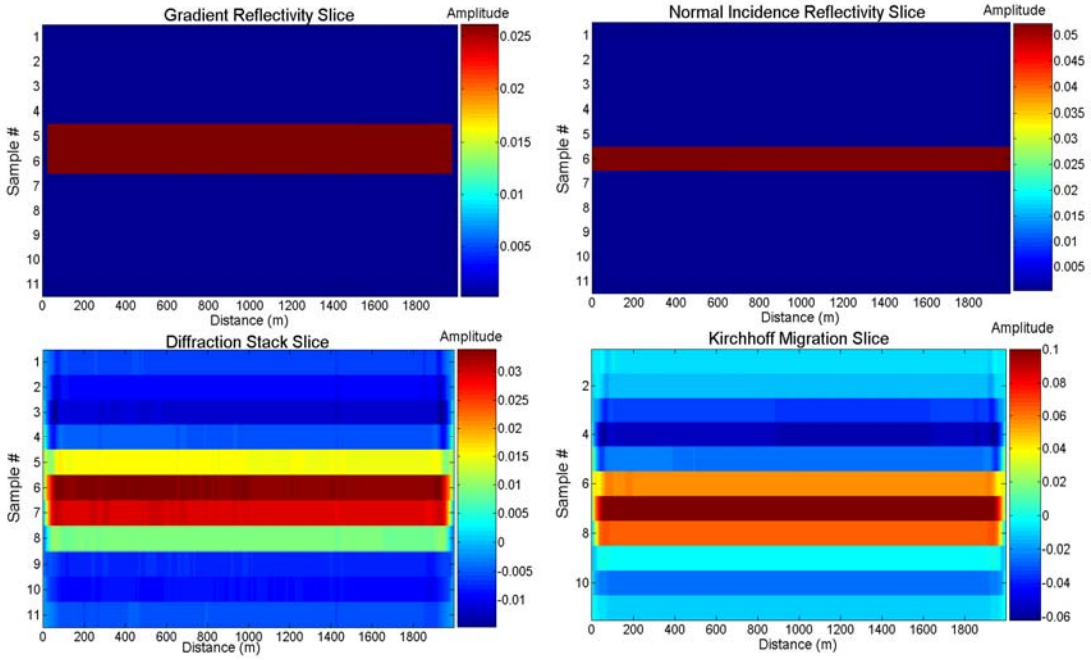

FIG. 10. Horizontal slice matrices through the first horizontal reflector in each reflectivity matrix.

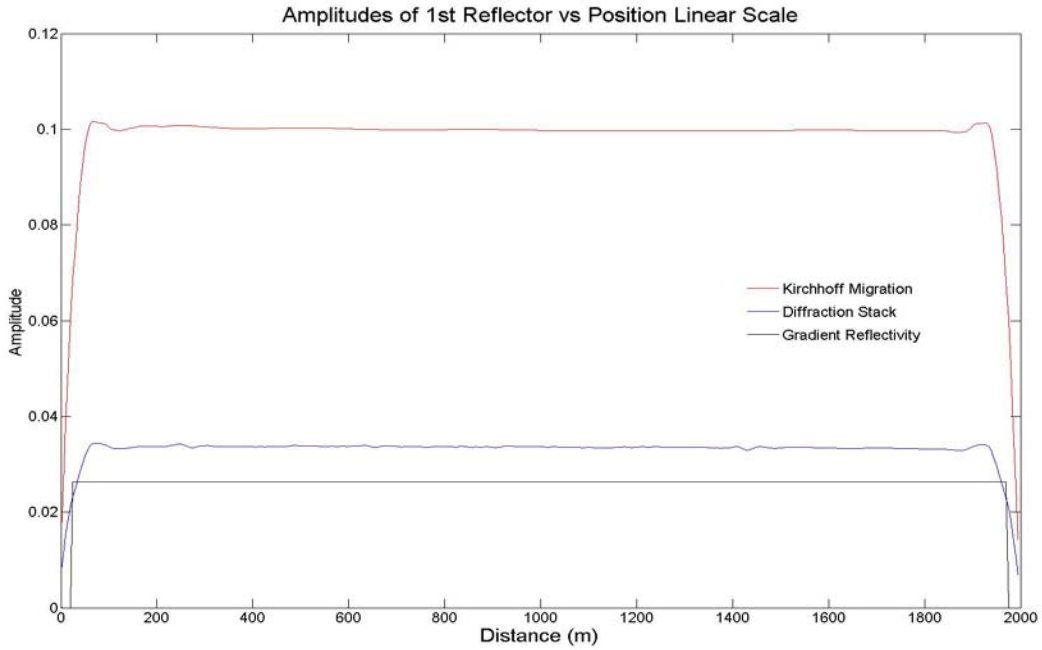

FIG. 11. Plot of peak amplitudes extracted from horizon slices through reflector 1. Kirchhoff migration amplitudes in red, diffraction stack in blue and gradient reflectivity in black.

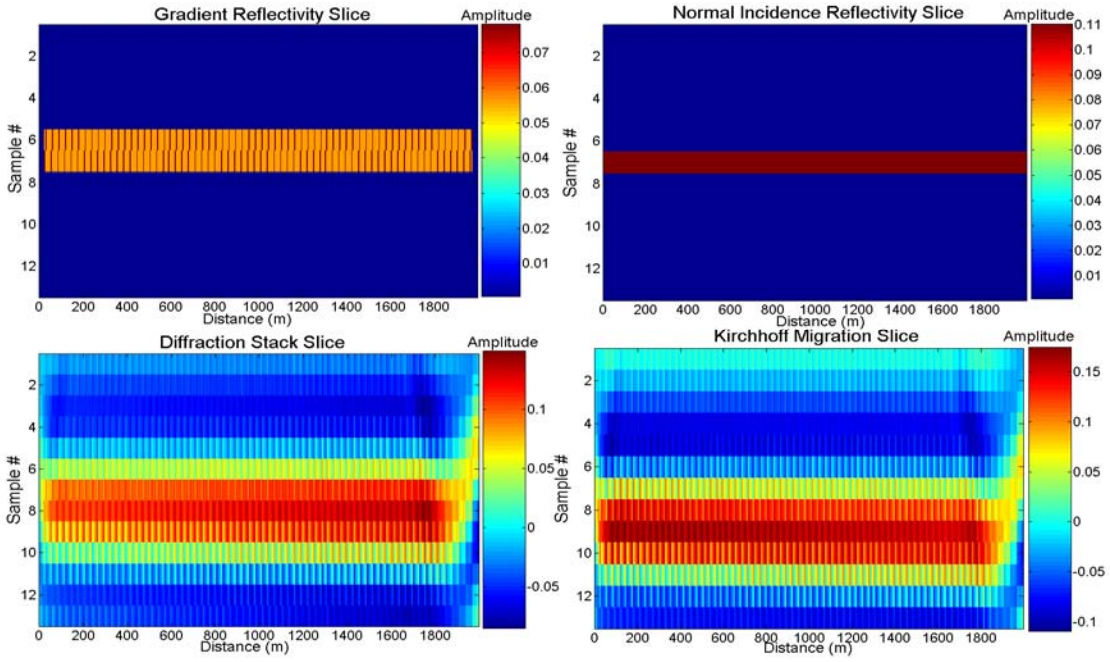

FIG. 12. Slice matrices through the 2nd dipping reflector in each reflectivity and migration matrix.

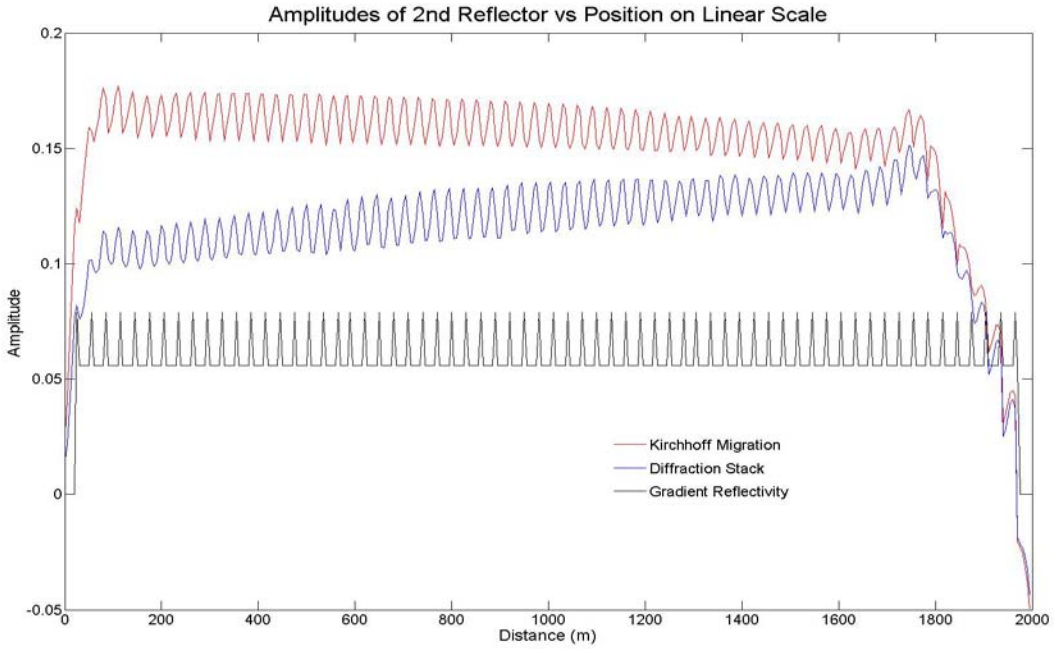

FIG. 13. Plot of peak amplitudes extracted from horizon slices through reflector 2. Kirchhoff migration amplitudes in red, diffraction stack in blue and gradient reflectivity in black.

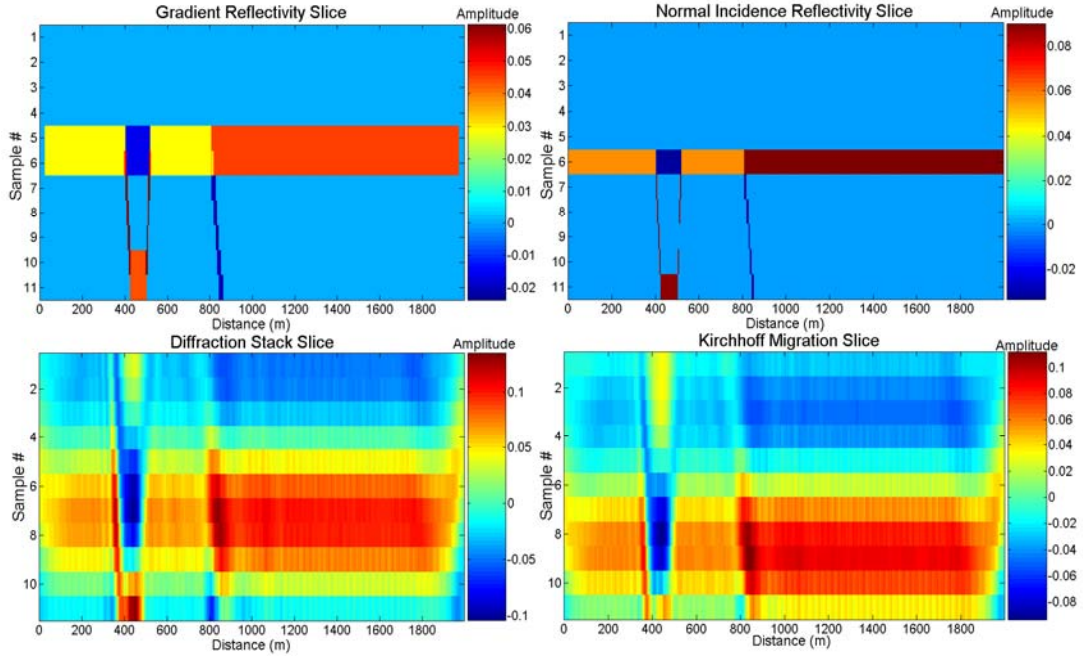

FIG. 14. Slice matrices through the 3rd reflector in each reflectivity and migration matrix.

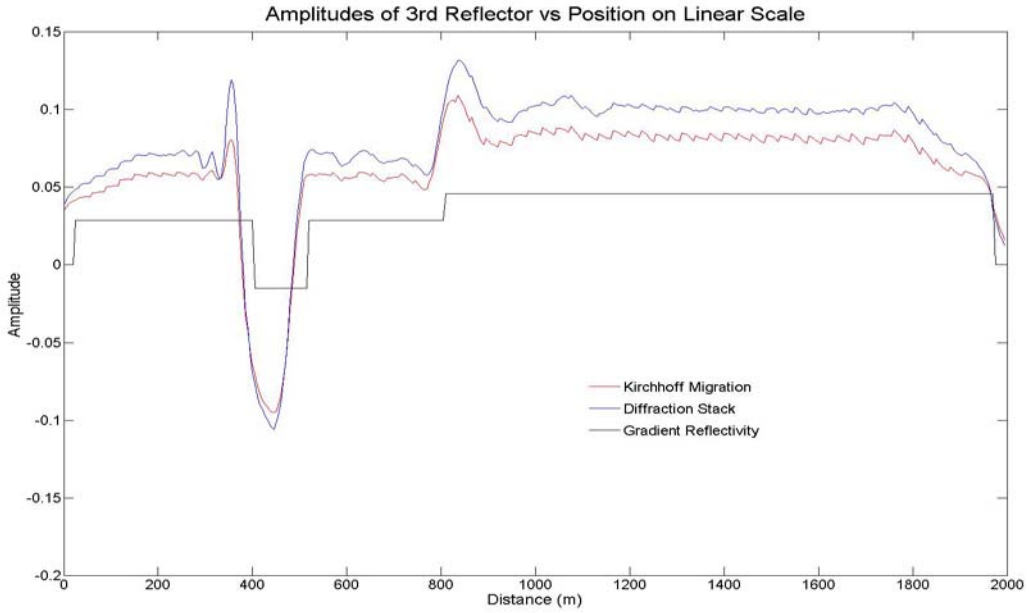

FIG. 15. Plot of peak amplitudes extracted from horizon slices through reflector 3. Kirchhoff migration amplitudes in red, diffraction stack in blue and gradient reflectivity in black.

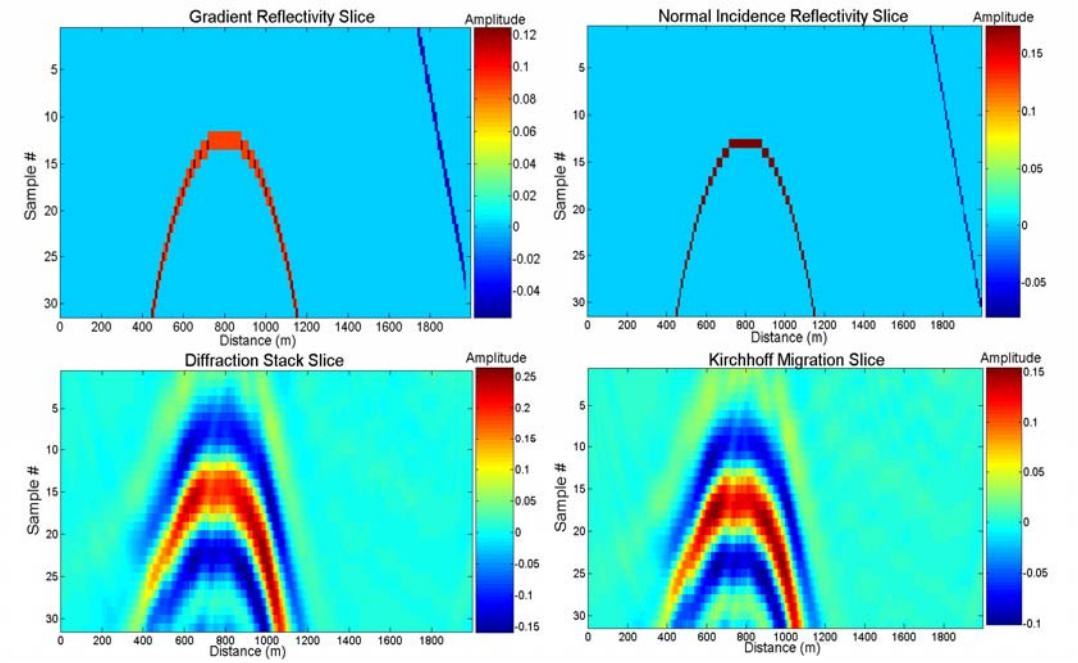

FIG. 16. Slice matrices through the antiformal reflector in each reflectivity and migration matrix.

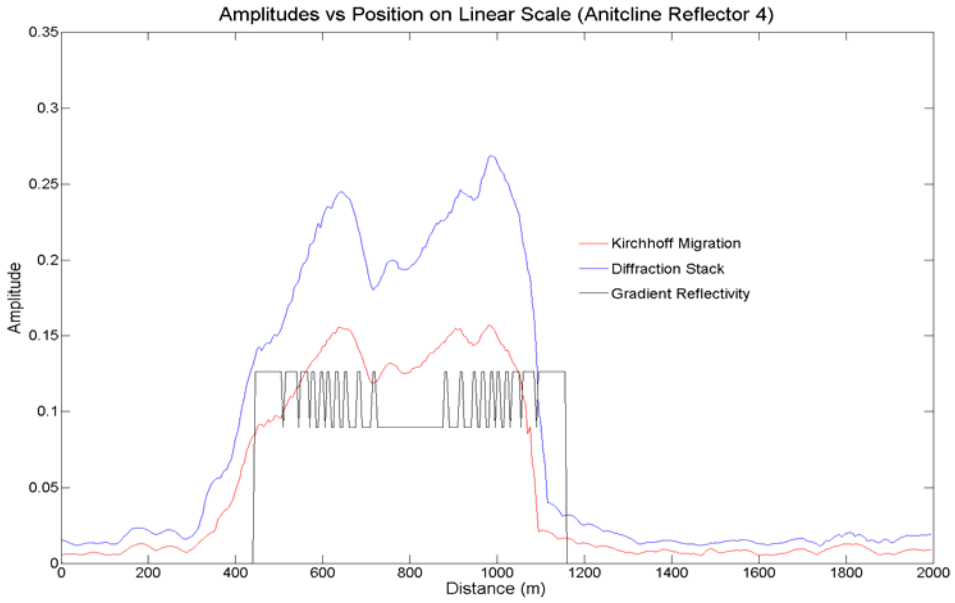

FIG. 17. maximum amplitudes from each column in the anticline slices vs. position. Kirchhoff migration amplitudes in red, diffraction stack in blue and gradient reflectivity in black.

Next the mean value of each reflectivity estimate was calculated from these extractions on well chosen intervals that excluded the edge values, namely from about 200 to 1800m for reflectors 1 through 3 and from about 450m to 1100m for the values from the anticline reflector 4 amplitude extractions. These mean values are collected in Table 2 below.

Table 2. Mean values of peak amplitudes from Reflectors 1-4 in Migration and Reflectivity Matrices.

	Kirchhoff Migration	Diffraction Stack	Gradient Reflectivity	Normal Incidence Reflectivity
Reflector 1 Mean	0.09991	0.03359	0.02634	0.05263
Reflector 2 Mean	0.15920	0.12324	0.05962	0.11111
Reflector 3 Mean	0.06424	0.07920	0.03576	0.07134
Reflector 4 Mean	0.13146	0.21515	0.10504	0.17647

Finally the amplitude contrast between the reflectors is compared by dividing the mean value of the stronger reflector by the mean value along the weaker reflector as in equation 19. Here we define the reflector contrast as

$$contrast = \frac{mean\ amplitude\ stronger\ reflector}{mean\ amplitude\ wea\,\mathrm{ker}\,reflector} \tag{19}$$

Table 3. Contrast between reflector mean amplitudes in each reflectivity matrix.

Contrast	Normal Incidence	Gradient Reflectivity	Kirchhoff Migration	Diffraction Stack
Reflector 2:Reflector 1	2.11111	2.26363	1.59339	3.66866
Reflector 4:Reflector2	1.58824	1.76172	0.82573	1.74584
Reflector4:Reflector 1	3.35294	3.98789	1.31572	6.40488

From Table 3 we see that the contrast between the reflectors has in general been decreased in the Kirchhoff migration image whereas these contrasts in amplitude have been increased in the diffraction stack image as compared with the gradient reflectivity. The amount of this increase and decrease may be quantified by comparing it to the contrasts in the gradient reflectivity. Here we define the dynamic range expansion factor α to be

$$\alpha = \frac{Contrast\ in\ \mathrm{Im}age\ reflectors}{Contrast\ in\ \mathrm{mod}el\ reflectors} \tag{20}$$

In a best case scenario α =1 and there is no change in the dynamic range between the model and the inverted data. This value is calculated for each of the contrasts between reflectors as given in Table 3, and collected in Table 4 below.

Table 4. Dynamic range expansion factors for both migration methods for different reflectors.

α	Kirchhoff Migration	Diffraction Stack
Reflector 2:Refelector 1	0.70391	1.62070
Reflector 4:Reflector 2	0.46871	0.99098
Reflector 4:Reflector 1	0.32993	1.60608

Here we see that the Kirchhoff migration method generally decreased contrasts between the reflectors by a factor anywhere between 1.4 to 3 times, hence compressing the dynamic range of the image as compared with the gradient reflectivity. On the other hand the diffraction stack migration method either increased the contrast between reflectors by 1.6 times or held it nearly constant thus expanding the dynamic range of the image.

CONCLUSIONS

In this paper we tested two migration algorithms to determine their relative effects on the output amplitudes in the migrated images given specific model input reflectivities derived from the test velocity model. The two algorithms tested were a simple diffraction stack algorithm **difstack**, and a fully featured CREWES Kirchhoff migration algorithm **kirk_mig** with linear interpolation, and default settings. A least squares scale factor of 318.04 was computed for the Kirchhoff migration image and a scale factor of 0.02389 was computed for the diffraction stack image. Once normalized by these scale factors, amplitude slices were made through four key horizons and the peak amplitudes from the migration images directly compared to the reflectivities that produced them. It was found that the diffraction stack reflectivity estimates best fit reflectors 1 and 2 while the Kirchhoff migration reflectivity estimates had a closer fit to the gradient reflectivity for reflector 3 and the anticline reflector 4. Reflector contrast was defined and calculated for the mean values of reflector pairs in each reflectivity matrix. Finally the dynamic range expansion factor was defined and calculated for reflector pairs in both the Kirchhoff migration image and for the same pairs in the diffraction stack image. It was found from this expansion factor that the Kirchhoff migration method seemed to compress the dynamic range of the amplitudes by anywhere from 1.4 to 3 times whereas the diffraction stack method tended to expand the dynamic range by about 1.6 times. It was also seen that the Kirchhoff migration method produces amplitudes which are more constant and even as a function of position, whereas the amplitudes of the diffraction stack were seen to be more uneven erratic and varying as a function of position. It was also demonstrated that both methods are sensitive to abrupt lateral changes in reflectivity.

The workflow presented in this paper for quantitative post-stack migration amplitude comparison consisted of the calculation of the reflectivity, depth conversion of the migrated images, determination of the least squares scale factor, scaling the images by this scale factor to determine reflectivity estimates, matrix slicing and horizon amplitude extractions, careful selection of the bounds on which to compare these reflectivity estimates, and the determination of reflector contrast and dynamic range expansion effects. These techniques may be applied to the amplitude analysis of other post-stack

migration algorithms, and may be modified in for the analysis of pre-stack migration algorithms including industrial migration algorithms.

FUTURE WORK

Future research will focus on extensions of the test methodologies presented in this paper to 2D and 3D prestack migration algorithms, including Fourier domain methods such as the Gazdag phase shift method, and time domain finite difference methods such as reverse time migration and one way 15 degree finite difference method. Both time and depth migrations will be tested with varying parameters including random noise, and shot receiver geometries. Finally industrial versions of the aforementioned migration methods will be tested.

ACKNOWLEDGEMENTS

We would like to thank Dr. Chuck Ursenbach from the University of Calgary, for his additional assistance. We would also like to thank the CREWES sponsors for their sponsorship of the CREWES project and for their passion for the earth sciences.

REFERENCES

Bancroft, J.C., A Practical Understanding of Pre- and Post Stack Migrations, (2006), SEG Course Notes.

CREWES MATLAB toolbox, (2006), CREWES

Krebes, E.S., Geophysics 551 Seismic Theory and Methods, Course Notes, 2nd Ed. (2006), University of Calgary, Department of Geology and Geophysics

Margrave, G.F., Numerical Methods of Exploration Seismology, (2003), University of Calgary, Department of Geology and Geophysics

Margrave, G.F., Methods of Seismic Data Processing, Geophysics 557/657 Course Lecture Notes, (2005), University of Calgary, Department of Geology and Geophysics

Schneider, W.A., Integral Formulation for Migration in Two and Three Dimensions, (1978), Geophysics, Vol. **43**, No1 (February 1978); P. 49-76.